X-ray Excited Optical Luminescence from Hexagonal Boron Nitride Nanotubes: Electronic Structures and the Role of Oxygen Impurities

Lijia Liu,[†] Tsun-Kong Sham,[†,*] Weiqiang Han,[‡] Chunyi Zhi,[§] and Yoshio Bando[§]

[†]Department of Chemistry, University of Western Ontario, London, Ontario, N6A 5B7 Canada, [‡]Center for Functional Nanomaterials, Brookhaven National Laboratory, Upton, New York 11973, United States, and [§]International Center for Materials Nanoarchitectonics (MANA), National Institute for Materials Science (NIMS), 1-1 Namiki, Tsukuba, Ibaraki 305-0044, Japan

ABSTRACT We report a study on the optical luminescence properties and the electronic structures of boron nitride nanotubes (BNNTs). BNNTs with natural B (80% ^{11}B and 20% ^{10}B) and pure ^{10}B are investigated in comparison with hexagonal BN crystals using X-ray absorption near-edge structures (XANES) and X-ray excited optical luminescence (XEOL). We find that the BNNT specimen synthesized with natural B contains more oxide impurities than that with pure ^{10}B, resulting in significantly different behavior in optical luminescence. All BN samples with hexagonal structures are found to emit strong luminescence, but the emission spectra are strongly morphology- and structure-dependent. XEOL and XANES measurements were carried out at the B K-edge, N K-edge, and O K-edge in order to reveal the origin of different luminescence channels and the corresponding electronic structures in these BN materials.

KEYWORDS: boron nitride nanotubes · X-ray absorption near-edge structures · X-ray excited optical luminescence · oxygen impurities

The boron nitride nanotube (BNNT) has attracted extensive interests in recent years due to its structural similarity with carbon nanotubes, but higher chemical and thermal stability.[1] It has a constant indirect band gap of 5.5 eV regardless of nanotube morphology (*e.g.*, diameters, helicity), which makes it a promising material for light-emitting devices.[2] Although several studies have been reported on the optical properties of hexagonal BN crystals and BN nanostructures using photoluminescence (PL) and cathodoluminescence (CL) techniques, the detailed luminescence spectra are slightly different depending on the excitation source and the morphology of the materials. It is commonly observed that BN exhibits two luminescence bands: a sharp, deep UV (~220 nm) emission and a broad UV−violet (~280−380 nm) emission;[3−6] the former is attributed to the near-band-gap excitonic emission, whereas the latter is normally attributed to the structural defect or the presence of impurities. The UV−violet emission is of particular interest as it is found to be strongly dependent on the purity and the morphology of BN. The emission at this region is usually shown as multiplets of equally spaced sharp peaks, especially at low temperature, which are due to the coupling between electrons and phonons (phonon replica).[5−7] It also has been found that luminescence at this region shows additional features either by introducing oxide impurities[8] or under external stimulation.[9] Though various studies have been carried out on the luminescence of hexagonal BN, studies on BN nanotubes are still lacking and the luminescence mechanism of the B−N system is still unclear. In this paper, we study the correlation between luminescence and the electronic structure of BNNTs using X-ray absorption near-edge structures (XANES) and X-ray excited optical luminescence (XEOL), unlike conventional PL and CL measurements, of which the energy of the excitation source is often limited within the UV−visible region and *via* secondary processes following electron energy loss, respectively. In our study, tunable X-ray provided by synchrotron radiation is used to selectively excite the core electrons of B and N in BN and the accompanying luminescence during de-excitation is monitored while the photon energy is scanned across an absorption threshold (edge). We found that, under X-ray excitation, BN emitted bright violet light with unique features depending on the specific electronic structure of the sample.

XANES measures the X-ray absorption coefficient from a few electronvolts below

*Address correspondence to tsham@uwo.ca.

Received for review October 25, 2010 and accepted December 9, 2010.

Published online December 23, 2010. 10.1021/nn102881j

to ~50 eV above the absorption threshold of a core electron being excited into the unoccupied bound and quasi-bound states in a chemical environment following the dipole selection rule. It is element- and site-selective and can be used to distinguish the chemical bonding in the local environment of an atom in a material (*e.g.*, π*-like, σ*-like bonds).[10] Because BN is structurally graphite-like, the B and N are sp^2 hybridized, showing a strong 1s → π* transition at the B and N K-edges. Previous studies have been done to analyze the distributions of different BN crystal phases in BN film based on the contribution of the sp^3 and sp^2 bond contents.[11,12] XANES has also been used to study BN nanotubes, and it was found that it is also sensitive to the curvature of the nanotubes and the presence of impurities.[13] In the soft X-ray region, XANES is obtained by monitoring the total electron yield (TEY) and X-ray fluorescence yield (FLY). TEY measures the photoelectrons, Auger electrons, and other secondary electrons emitted from the sample under X-ray excitation, providing surface sensitivity (a few nanometers for BN). FLY, on the other hand, is more bulk-sensitive (hundreds of nanometers), depending on the attenuation length of the fluorescence X-ray from B and N.

XEOL measures the light emission (200−900 nm) from materials upon X-ray excitation. It is an X-ray photon in, optical photon out technique, which can be used to monitor the luminescence response with selected excitation energy.[14] The intensity of the luminescence is dependent on the portion of the absorbed energy that is transferred to the optical de-excitation channel. Also, by tuning the excitation energy across the absorption edge of the element of interest in the material, one can measure the photoluminescence yield (PLY) simultaneously with XANES to find out whether or not a given element or site is responsible for the luminescence. For sample, with multiple luminescence channels (multiple peaks in XEOL spectra), the PLY can be collected using a selected wavelength range (optical window) to reveal the origin of the luminescence.[15]

Recently, Han *et al*. investigated the luminescence from BNNTs upon B isotope substitution using CL.[16] A broad 4 eV emission with a sharp 3.31 eV peak was observed from the BNNT of natural B (80% ^{11}B and 20% ^{10}B), whereas three sharp peaks at 3.76, 3.92, and 4.09 eV were observed from the ^{10}B-substituted BNNT. They have tentatively attributed the differences in the two CL spectra to the different levels of oxide contaminations in the materials. It is surprising that the difference in light-emitting properties is significant in the two BNNT materials; therefore, whether or not it is caused by isotope substitution or impurity is worth investigating. Thus, in this study, we investigate the luminescence of the same materials: BNNTs with and without B isotope substitution studied previously[16] using XANES and XEOL at the B, N, and O K-edges. The results are compared with those of bulk hexagonal BN crystals.

RESULTS AND DISCUSSION

Electronic Structure of BN. Figure 1 shows the XANES spectra of hex-BN, nat-BNNT, and 10-BNNT at the B K-edge and the N K-edge. All spectra are normalized to the unit edge jump and shifted vertically for clarity. The B K-edge TEY spectra are shown in Figure 1a. Characteristic features of the sp^2 hybridized B−N system can be seen from all BN samples: the intense sharp peak a at 192 eV is the B 1s to π* transition; the doublet peak (c and d) at 198.2 and 199.5 eV and the weak resonances f (204.5 eV) and g (215.9 eV) are features from the B 1s to σ* transition.[11] However, in nat-BNNT, a sharp peak b, located at 194 eV, becomes the most intense peak, and the fine features belonging to the BNNT (peaks f and g) are buried under a broad resonance, e, centered at 203 eV. Peaks b and e are attributed to oxide impurities, as they show exactly the same features as what is seen from B_2O_3. On the other hand, 10-BNNT appears oxide-impurity-free, as it shows identical features as those in hex-BN.

Similar results are also observed from FLY spectra (Figure 1b), in which nat-BNNT shows the resonances characteristic of B−O bonding, whereas the other two are BN of sp^2 hybridization and free of oxide. This observation indicates that the samples are optically thin, showing no obvious saturation effect. The intensity ratio of peaks a and b is increased in FLY, indicating that there is less oxide at the bulk than on the surface. Because the oxide feature is still relatively intense in the spectra (*i.e.*, peak b is stronger than peak a), the oxide is not just on the surface but also present in the bulk of the BNNT. The π* transition (peak a) in FLY is broadened compared with the peak in TEY for the two BNNTs, but the broadening is less obvious for bulk hex-BN. The broadening of the π* peak in BNNTs relative to hex-BN could be attributed to the removal of the degeneracy of the π* band as the overlapping of p_z orbitals in the nanotubes is increased due to the small tube curvature.[17] The multiwalled nanotube structure creates differences in the outer and inner tube diameters. The fact that only FLY shows peak broadening means that it has a stronger effect at the inner side of the BNNTs. It is interesting to note that FLY of the nanotubes shows a larger π*/σ* ratio, that is, that peak a is more intense in FLY relative to TEY. The TEY signal mostly comes from the sample surface, where the B−N plane is less constrained and more susceptible to ambient gas adsorption, whereas FLY is able to probe inner tubes with increasing constraints.

The N K-edge TEY and FLY XANES are shown in Figure 1c,d, respectively. From TEY of hex-BN, we can see that the spectrum is composed of a sharp peak, a, at 402.6 eV, which is the N 1s to π* transition, and several other peaks, b (407 eV), c (409.2 eV), and e (416.6 eV), which are the N 1s to σ* transitions.[18] Similar features are seen in FLY with some attenuation due to self-absorption[19] because the photon energy at the N

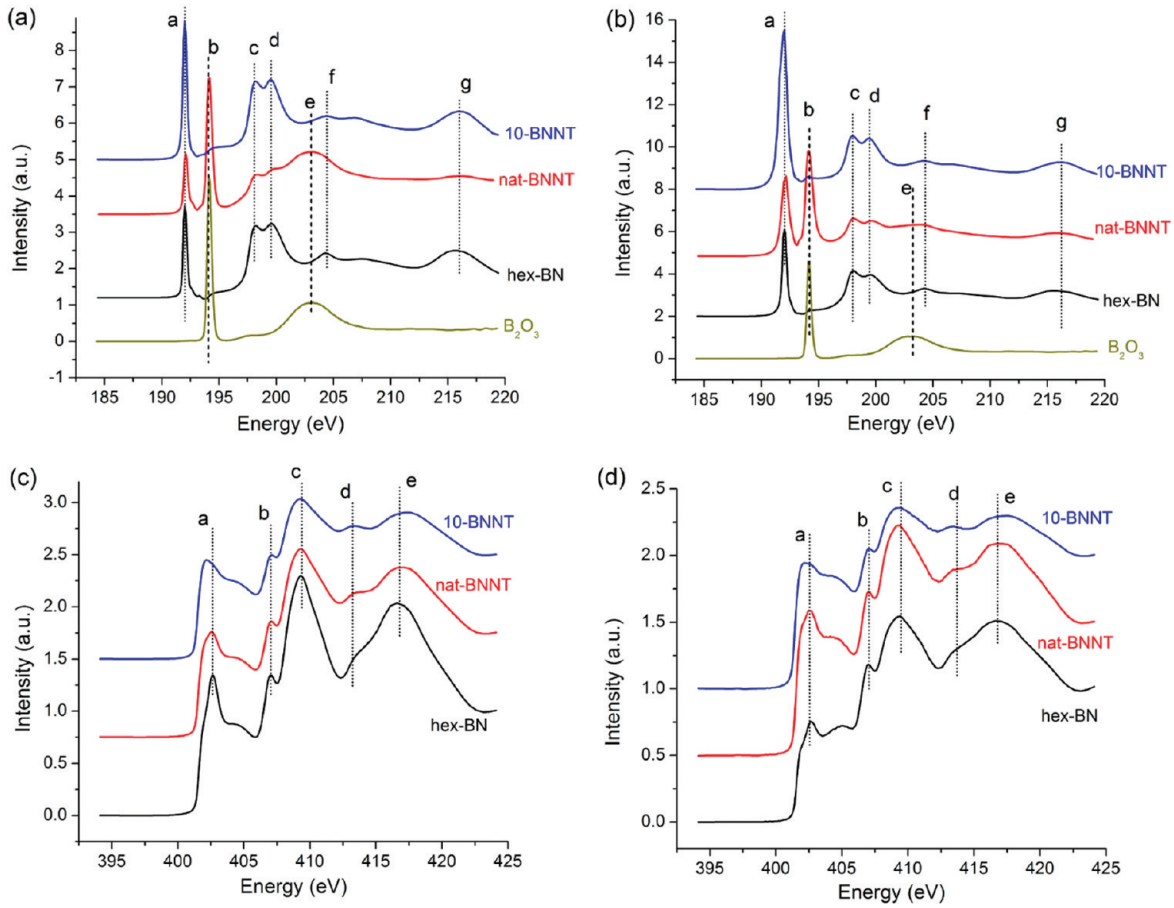

Figure 1. XANES of hex-BN, nat-BNNT, and 10-BNNT. (a) B K-edge TEY, (b) B K-edge FLY, (c) N K-edge TEY, and (d) N K-edge FLY. The XANES of B_2O_3 at the B K-edge was also included as a reference in (a) and (b).

K-edge has a larger penetration depth than at the B K-edge and the fluorescence from N can be reabsorbed by B. If we look at peak a closely, we find that the feature at 402.1 eV, which is seen as a shoulder in hex-BN, becomes more intense in nat-BNNT and dominates in 10-BNNT. The 0.5 eV energy down-shift of the N 1s $\rightarrow$ π^* transition has also been observed from other BN nanostructures and is attributed to the curvature effect from the BN honeycomb layers.[13,17,20] Another peak shift from bulk BN to nano BN is the blue shift of peak e, which is 0.5 eV higher in 10-BNNT than in hex-BN. A slightly increased intensity of peak d is also observed from 10-BNNT.

The above observations show that, although synthesized *via* the same route, BNNTs prepared with and without B isotope differ in purity. The 10-BNNT has a better curvature feature with no noticeable oxide impurities, whereas nat-BNNT is rich in surface oxide forming B−O bonding, which, however, has little effect on the conduction band modification at the N K-edge. The reason for this is not entirely clear and may be due to the kinetics, which segregates the N from the B−O interaction. As the proposed reaction mechanism for BNNT synthesis involves the formation of the B_2O_2 molecule,[21] it may further grow into a B_nO_m cluster, forming a B−O ring structure substituting the B−N network.[22]

Luminescence from BN. Figure 2a shows the XEOL spectra with selected excitation energies from below to above the B K-edge. The XEOL excited at the N K-edge shows the same profile thus not shown. It can be seen that the luminescence from hex-BN covers a broad range of the spectra from 2.5 to 4.8 eV. The highest emission intensity is located between 3.75 and 4.09 eV, and the emission is composed of several small oscillations. The other emission band at 3.2 eV (387.5 nm) with less intensity is shown as a shoulder to the main peak. The luminescence exhibits strong intensity both below and far above the B K-edge, but it decreases drastically at the edge resonance, leading to an inversion. We shall return to this point later. It should be noted that, although the intensity of the luminescence varies with different excitation energies, the normalized spectra show that the relative ratio of the two components remains the same regardless of the excitation energy (Figure 2b), indicating that the two features may have a similar luminescence mechanism. If we take a closer look at the main emission peak, we can clearly see that the peak is composed of three oscillations that are almost equally spaced. These oscillations are associated with lattice vibrations of the B−N network. The 3.87 and

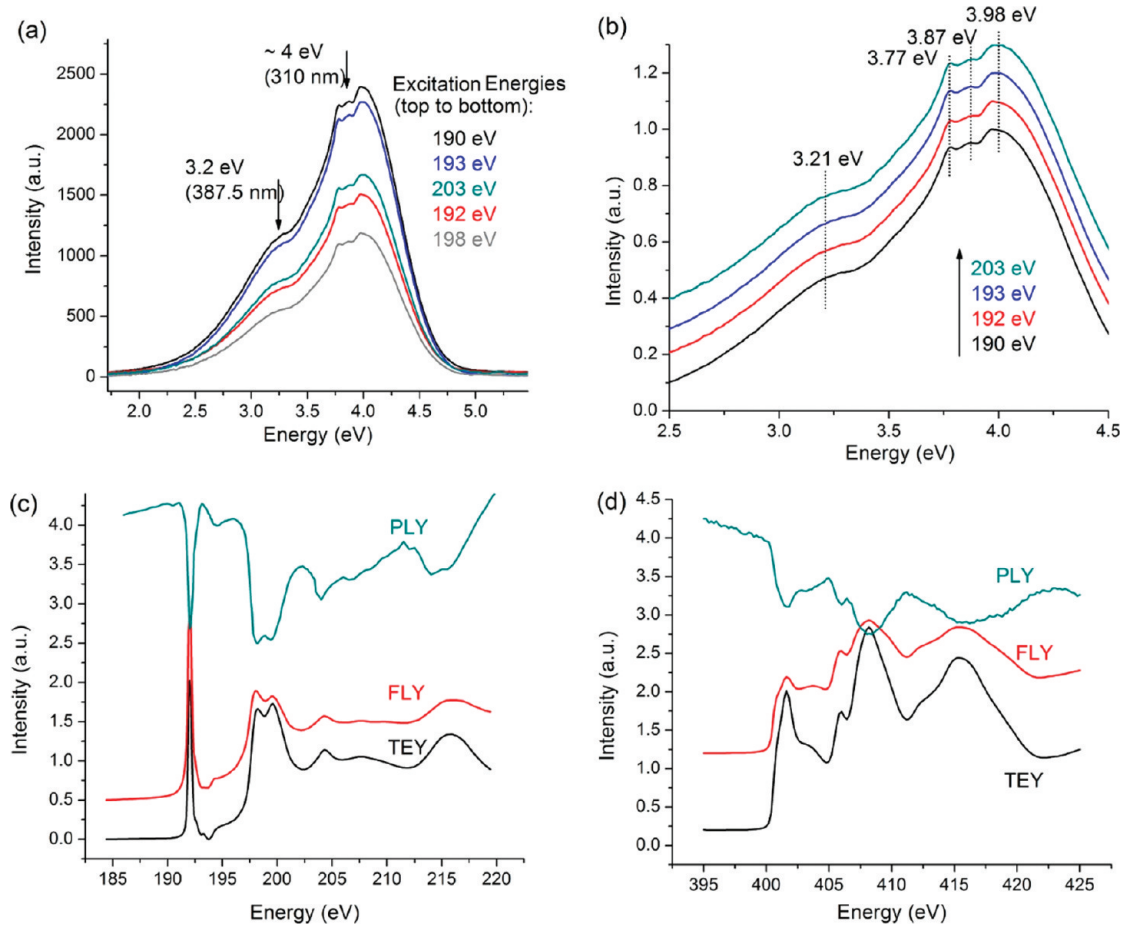

Figure 2. (a) XEOL spectra of hex-BN at selected energies from below to above the B K-edge. (b) Enlarged view of the main emission peak after normalization and being shifted vertically for clarity. (c) PLY (zero-order)-XANES of hex-BN at the B K-edge. (d) PLY(zero-order)-XANES of hex-BN at the N K-edge.

3.77 eV peaks are the first- and second-order phonon replica of the 3.98 eV emission. The phonon replica is quite commonly observed in groups III−V semiconducting materials, such as GaN, where the donor−acceptor pair recombination is assisted by phonons to facilitate the light emission.[23] Similar results have been observed from hexagonal BN using PL and CL.[6,24] The intervals between the peaks are caused by energy dissipation of the B−N A_{2u} vibration band (~800 cm^{-1}), which has been observed from infrared spectra.[16,25,26]

We now turn to the variation of luminescence intensity across the absorption edge, shown as PLY spectra with the excitation energy scanned across the B and N K-edges in comparison with the XANES spectra (Figure 2c,d). The zero-order PLY at both B and N K-edges shows all the resonances observed in XANES, but completely inverted; that is, the luminescence from hex-BN decreases significantly once the photon energy is tuned to the absorption edge of the core electron. This means that the luminescence intensity of hex-BN is sensitive to how the incoming photon is absorbed for both B and N. At energies below the edge, the absorption coefficient is relatively small; only electrons at shallower levels (valence and shallow inner shell electrons) are able to be prompted to the unoccupied electronic states, resulting in the electron−hole pair recombination *via* the optical channel. Once the photon energy is tuned to the edge of the core electron, the penetration depth of the incident photon abruptly decreases due to a sharp jump in the absorption coefficient. A main fraction of the Auger electron and fluorescence X-rays that are responsible for producing secondary electron−hole pairs *via* thermalization can escape the solid without transferring the energy to the optical channel. The decrease in quantum yield of the optical photons is caused by the shortening of the probing depth at both edges; thus, the observed luminescence is likely due to the bulk defect of hexagonal BN crystals.

The XEOL spectra of nat-BNNT exhibit features that are significantly different from those of hex-BN, as shown in Figure 3a. The main emission is composed of two sharp features located at 4.05 and 3.89 eV, a shoulder at 3.78 eV, followed by several weak oscillations toward lower energy, and a broad emission at 3.0 eV, which is much weaker than the 3.2 eV emission from hex-BN. Also, unlike hex-BN, the emission reaches the highest intensity at the edge (192 eV), while the low-

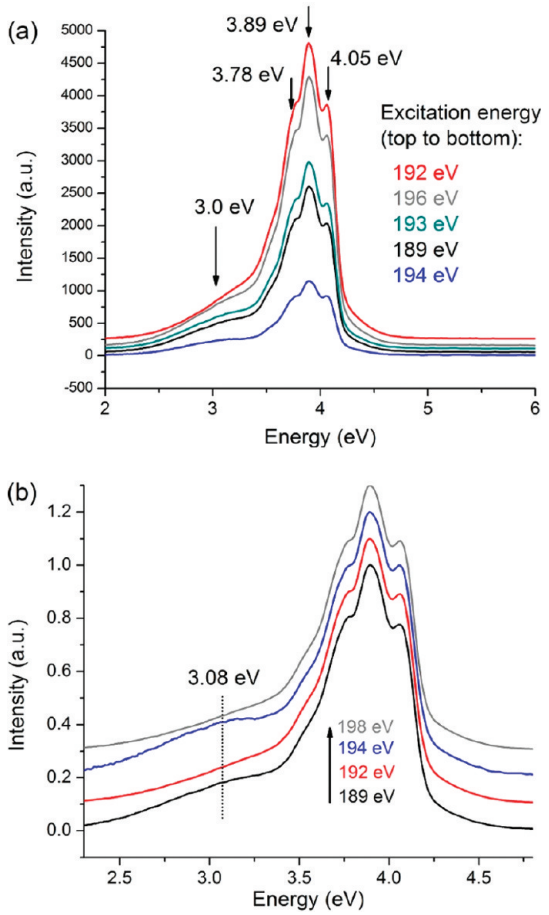

Figure 3. (a) XEOL of nat-BNNT with selected excitation energies across the B K-edge. (b) XEOL with intensity normalized to the 3.89 eV emission and shifted vertically for clarity.

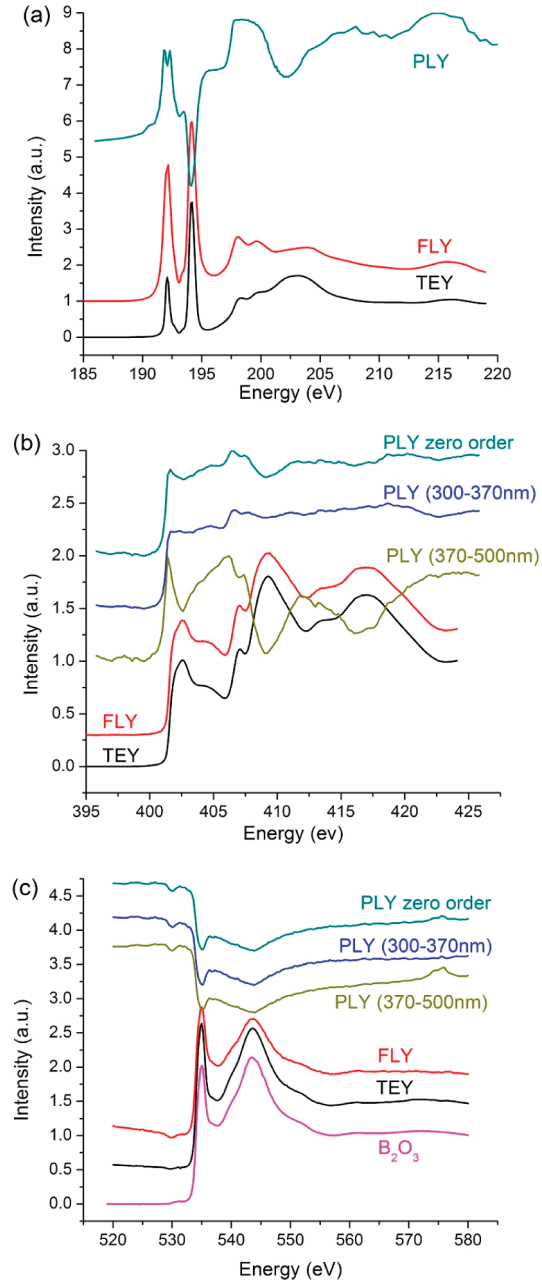

Figure 4. PLY-XANES of nat-BNNT at the (a) B K-edge, (b) N K-edge, and (c) O K-edge. B_2O_3 TEY is shown as a reference.

est emission is observed upon excitation at the edge of B in the B−O environment (194 eV). It is also interesting to look at the normalized spectra (Figure 3b). In this case, the 4 and 3 eV emissions behave differently, as indicated by the variation of the intensity ratio between the two regions. After normalization to the 3.89 eV peak, we can see that the 3 eV emission shows the lowest intensity at 192 eV, which is at the B K-edge of BN, but becomes more intense once the oxide channel turns on (194 eV). PLY-XANES of the B K-edge in Figure 4a shows the variation of zero-order luminescence intensities across the edge. It can be seen that, unlike the inverted PLY observed from hex-BN, the PLY of nat-BNNT shows a combined feature of both B−N and B−O, and the former contributes to the luminescence positively, whereas the latter quenches the luminescence.

Wavelength selected PLY at the N K-edge is shown in Figure 4b, with optical windows set to monitor the main 4 eV luminescence (300−370 nm) and the 3 eV (370−500 nm) shoulder. We clearly see that the zero-order luminescence and the main emission peak within 300−370 nm show little variation above the edge. However, the weak emission at the 370−500 nm region displays all the features same as the absorption spectra with partial inversion. This suggests that the changing of absorption coefficient of N does not affect the 4 eV luminescence but modulates the 3 eV luminescence; thus, N contributes mainly to the weak 3 eV emission.

On the other hand, the O K-edge XANES shown in Figure 4c displays well-defined features that resemble the O K-edge XANES of B_2O_3, albeit inverted. This further confirms the presence of oxide in nat-BNNT. On comparison with TEY and FLY XANES, the PLY XANES across the O K-edge shows a strong dependence on the variation of the absorption coefficient regardless of the emission window selected; thus, both luminescence bands have a significant oxide contribution. All

PLY spectra are completely inverted at the O K-edge; this is mainly due to a significantly reduced quantum yield caused by O absorption at the O K-edge (as compared to B absorption at the B K-edge) as well as a saturation effect (penetration depth of soft X-ray is ~250 nm above the edge).

Compared with the XEOL of hex-BN, the XEOL of nat-BNNT differs significantly, especially in the 4 eV region. Unlike a broad peak with multiple phonon replicas in hex-BN, the emission from nat-BNNT shows as a sharp shoulder at 4.05 eV and the main peak at 3.89 eV, followed by oscillations toward the lower energy. The emission intensity (PLY spectra in Figure 4) is highly sensitive to the absorption across the B and O K-edges, but showing little change at the N K-edge, at which the luminescence intensity exhibits a positive edge jump, followed by a nearly constant response. The inverted PLY of the B and O K-edges indicates that the emission is quenched once the boron oxide channels open up. It should be noted that boron oxide itself shows no luminescence upon X-ray excitation. The crystal structure of boron oxide is commonly accepted as connecting triangle BO_3 units (α-B_2O_3),[27] whereas it is not the case for oxide impurities in nat-BNNT. In fact, oxide species can be considered as dopant in the B−N network, for example, substituting a B or N atom or a B−O moiety upon the formation of B−O six-membered rings.[22] The extra valence electron in O introduces a new impurities level that could recombine with holes in the valence band to produce an optical emission. Hence, the increase of absorption at the B site leads to an increase in optical yield at the B K-edge in the B−N environment. However, once the B sites in the B−O environment are preferentially excited at the B K-edge, the preferred decay is not *via* an optical channel; therefore, we see a significant decrease in luminescence intensity. The energy partially transfers to the B−N system that yields an increase in the 3.2 eV emission. The 4.05 eV shoulder emission should be thus attributed to the emission from the B−O impurity level. The 3.89 eV is caused by energy dissipation due to lattice stretching in the BNNT, as the interval between this peak and the 4.05 eV peak (1290 cm^{-1}) is close to the frequency of the B−N stretching mode (1376 cm^{-1}).[28] Other weak shoulders at energy lower than 3.89 eV should be assigned to a phonon replica, similar to what has been seen from hex-BN.

The XEOL of 10-BNNT is shown in Figure 5a. The luminescence consists of two peaks: one at 3.21 eV with higher intensity and the other at 3.76 eV. The positions of the emission peaks are actually quite similar to what has been observed from hex-BN (Figure 2a) with all peaks being narrower. The 3.76 eV emission is accompanied with two small oscillations at 3.85 and 3.96 eV, which is similar to the phonon replica features in hex-BN. However, these two emissions also exhibit unique features that are different from hex-BN: (1) the 3.76 eV

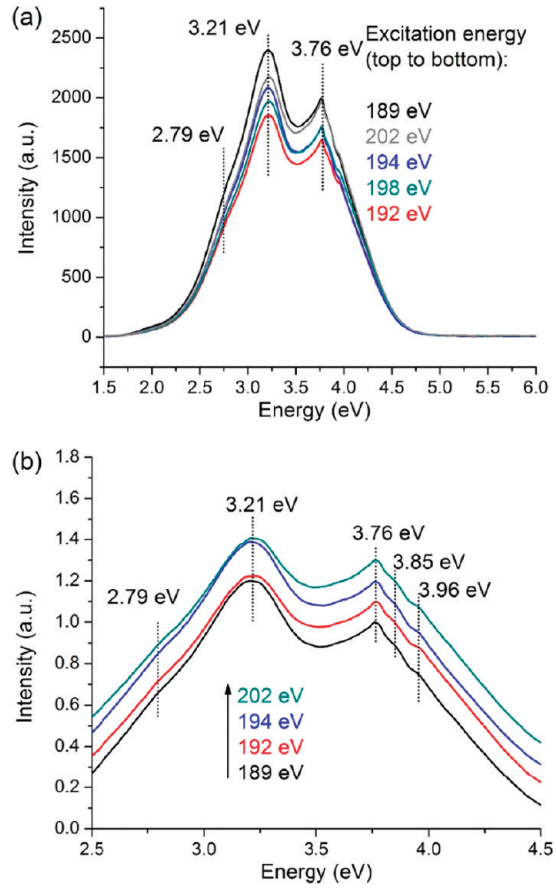

Figure 5. (a) XEOL of 10-BNNT with excitation energy across the B K-edge. (b) Enlarged view of XEOL at the 2.5−4.5 eV region after normalization to the 3.76 eV peak and being shifted vertically for clarity.

emission is the most intense peak of the three, whereas in hex-BN, the 3.98 eV is the strongest emission; (2) the 3.21 eV emission becomes the dominant emission in 10-BNNT. Moreover, the two emissions behave differently while tuning the excitation energy, as can be seen from the normalized spectra (Figure 5b). After normalization to the 3.76 eV peak, we can see that the relative peak intensity changes as the excitation energy goes from 192 to 194 eV. The 3.21 eV emission at 192 eV is less intense than that at 194 eV, which is similar to the trend of the 3.08 eV emission observed from nat-BNNT.

The PLY spectra of 10-BNNT also show several interesting features, as shown in Figure 6. At the B K-edge, the inverted PLY shows the resonances from BN with an additional peak at 194 eV (the B−O resonance), but no such peak shows up in either TEY or FLY. The N K-edge PLY displays the feature similar to the absorption spectra for both selected emission windows, indicating that both luminescences are N-related. If we take a look at the O K-edge spectra, shown in Figure 6c, the spectra show poor and noisy features due to low oxide concentration in the sample, but we can still see the weak oscillations from oxide. The zero-order PLY and PLY at the region of 370−450 nm exhibit weak responses across the edge, but the PLY at 300−370 nm

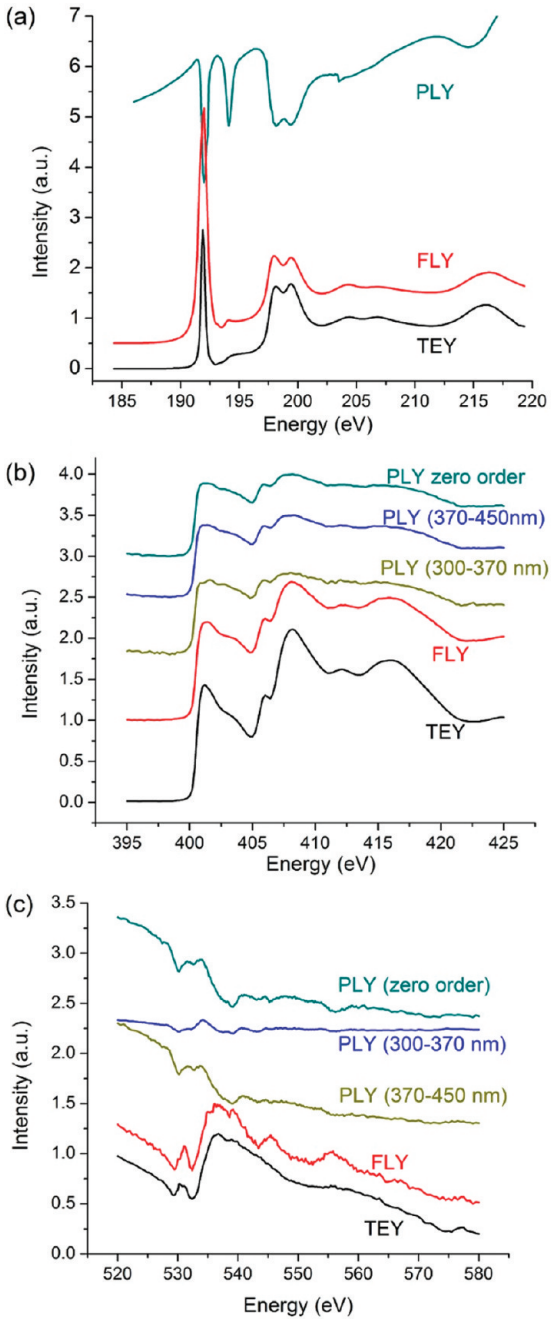

Figure 6. PLY-XANES of 10-BNNT at the (a) B K-edge, (b) N K-edge, and (c) O K-edge.

is almost flat. Thus, the presence of trace surface oxide affects the luminescence from the BNNT, particularly the emission in the 379−450 nm region. The oxide in this case is less likely the dopant, but rather just surface impurities, because the 4.05 and the 3.89 eV emissions are not observed. On the basis of these observations, the species could be a small BO^- molecule adsorbed on the surface, and it facilitates the energy transfer from B−O to B−N, enhancing the 3.21 eV emission (Figure 5b), which is similar to what has been observed from nat-BNNT (Figure 4b). Tang *et al*. also reported that, under UV irradiation, the adsorption of O on the BN surface could lead to the increase of the 3.2 eV emission.[8]

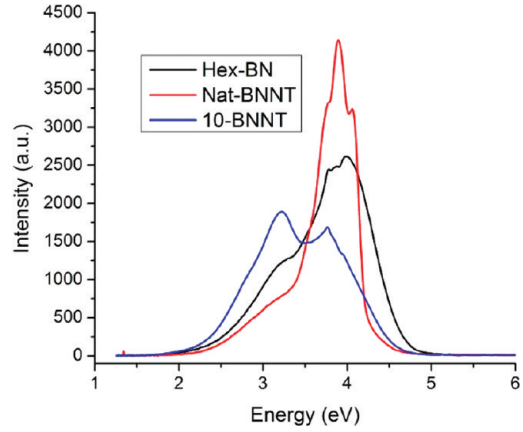

Figure 7. XEOL of hex-BN, nat-BNNT, and 10-BNNT with the excitation energy at 210 eV.

It is apparent from the above results that there are noticeable differences in both electronic structures and luminescence properties of nat-BNNT and 10-BNNT, especially in the B environment. The differences are caused by the amount of oxide impurities rather than the effect of isotope substitution. As we can see from the XANES spectra, both BNNTs show hexagonal B−N local structures that are the same as bulk BN crystallites. The most interesting observation is that the presence of oxide would significantly alter the luminescence properties of BN. Figure 7 compares the XEOL of all three BN samples with excitation energy at 210 eV. It can be seen that, though all BN materials studied here emit light in two wavelength regions (3 and 4 eV), the peak shape and the relative intensities vary considerably. It should also be noted that, though the emission band located at the 5−5.5 eV region is observed quite often by PL and CL, we did not see it in our case. It could either be due to the fact that it is the unfavorable decay channel upon X-ray excitation of core electrons or be due to an effective energy transfer pathway to the defect emission. The 3.2 eV emission is present in all BN samples regardless of size and oxide impurities, and the peak width is relatively broad with a similar profile, though the intensity is relatively weak in nat-BNNT compared with the main 4 eV emission. The 4 eV emis-

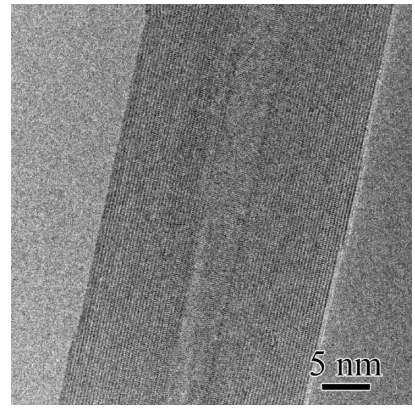

Figure 8. TEM image of an individual nat-BNNT.

sion, however, varies in shape upon formation of different defect levels, and this also indicates that the 4 eV emission has more than one origin, which are strongly dependent on the electronic structures.

CONCLUSION

We have examined the correlation between electronic structures and luminescence properties of three BN materials, hex-BN, nat-BNNT, and 10-BNNT, and the role of oxygen impurities. Our results clearly demonstrate the site-sensitivity of XEOL if different sites exhibit a large difference in the efficiency of the optical yield. Though sharing similar hexagonal structures as those of bulk crystals regardless of the B isotope, the BNNTs exhibit a unique optical emission at the deep blue-violet region upon X-ray excitation, and the presence of oxide impurities alter the emission spectra significantly. Several interesting findings are summarized below:

(1) Bulk hex-BN has a broad luminescence at 4 eV and a shoulder at 3.2 eV. Both emission bands are attributed to the bulk defect emission of different defect levels, and the 4 eV emission is also accompanied by a phonon replica.

(2) Nat-BNNT contains oxide impurities, and O atoms act as a dopant in BNNTs, which introduce new defect levels, resulting in the intense 3.89 eV emission. The 3.0 eV emission is from the bulk defect of BN, and the presence of oxide increases the intensity at this region *via* energy transfer once the oxide channel turns on.

(3) 10-BNNT is relatively free of oxide. The 3.76 eV emission is mainly from the intrinsic BN defect with a trace contribution from the surface oxide component. On the other hand, oxide impurities are mainly due to surface adsorption, which is responsible for the relative increase of the 3.2 eV emission due to energy transfer.

METHODS

The multiwalled BNNT was synthesized by reacting B powders with a mixture of MgO and SnO as precursors under an ammonia atmosphere. The details of the synthesis have been described elsewhere.[16,29] Isotope-substituted BNNTs were synthesized following the same route, replacing natural B powders with ^{10}B powders. Both BNNT samples have similar morphologies: 20−120 nm in diameter and several tens of micrometers in length, with wall numbers typically of tens. Figure 8 shows a transmission electron microscopy (TEM) image of a single nat-BNNT, with a diameter of 25 nm and a wall thickness of 10.2 nm. The natural BNNTs are, henceforth, denoted as nat-BNNT and BNNT with the B isotope are denoted as 10-BNNT. B_2O_3 powders (Sigma Aldrich) and BN powders of hexagonal crystal structures (Alfa Aesar) were also studied for comparison. The latter is, henceforth, denoted as hex-BN.

Synchrotron radiation measurements were carried out at the Canadian Light Source located at the University of Saskatchewan involving two beamlines providing different photon energy ranges. The Variable Line Spacing Plane Grating Monochromator (VLS-PGM) beamline with an energy range of 5−250 eV was used for the B K-edge measurements,[30] and the Spherical Grating Monochromator Beamline (SGM) with an energy range of 250−2000 eV is used for the N and O K-edge measurements.[31] The detection modes used at the two beamlines are the total electron yield (TEY), which records the specimen currents, and the X-ray fluorescence yield (FLY), using a multichannel plate.[32] XEOL was collected with a dispersive optical spectrometer (Ocean Optics, QE65000) while the excitation energy was tuned across the absorption edge. The photoluminescence yield (PLY) was also measured by collecting the total luminescence at zero order (200−900 nm) or at selected wavelength ranges while tuning the photon energy across the edge. All spectra were normalized to the incident photon flux measured with a refreshed Au mesh.

Acknowledgment. Research at the University of Western Ontario is supported by NSERC, CRC, CFI, and OIT. The Canadian Light Source, where the synchrotron measurements were conducted, is supported by CFI, NSERC, NRC, CHIR, and the University of Saskatchewan. The authors would like to thank beamline scientists L. Zuin, C. Ryan (VLS-PGM beamline), and T. Regier (SGM beamline) for their technical support at the Canadian Light Source. W.H. thanks the U.S. DOE, under contract DE-AC02-98CH10886, for its support.

REFERENCES AND NOTES

1. Rubio, A.; Corkill, J. L.; Cohen, M. L. Theory of Graphitic Boron Nitride Nanotubes. *Phys. Rev. B* **1994**, *49*, 5081–5084.
2. Blase, X.; Rubio, A.; Louie, S. G.; Cohen, M. L. Stability and Band Gap Constancy of Boron Nitride Nanotubes. *Europhys. Lett.* **1994**, *28*, 335–340.
3. Jaffrennou, P.; Barjon, J.; Lauret, J.-S.; Maguer, A.; Golberg, D.; Attal-Tretout, B.; Ducastelle, F.; Loiseau, A. Optical Properties of Multiwall Boron Nitride Nanotubes. *Phys. Status Solidi B* **2007**, *244*, 4147–4151.
4. Jaffrennou, P.; Barjon, J.; Schmid, T.; Museur, L.; Kanaev, A.; Lauret, J.-S.; Zhi, C. Y.; Tang, C.; Bando, Y.; Golberg, D.; et al. Near-Band-Edge Recombinations in Multiwalled Boron Nitride Nanotubes: Cathodoluminescence and Photoluminescence Spectroscopy Measurements. *Phys. Rev. B* **2008**, *77*, 235422.
5. Museur, L.; Feldbach, E.; Kanaev, A. Defect-Related Photoluminescence of Hexagonal Boron Nitride. *Phys. Rev. B* **2008**, *78*, 155204.
6. Silly, M. G.; Jaffrennou, P.; Barjon, J.; Lauret, J. S.; Ducastelle, F.; Loiseau, A.; Obraztsova, E.; Attal-Tretout, B.; Rosencher, E. Luminescence Properties of Hexagonal Boron Nitride: Cathodoluminescence and Photoluminescence Spectroscopy Measurements. *Phys. Rev. B* **2007**, *75*, 085205.
7. Berzina, B.; Trinkler, L.; Krutohvostov, R.; Williams, R. T.; Carroll, D. L.; Czerw, R.; Shishonok, E. Photoluminescence Excitation Spectroscopy in Boron Nitride Nanotubes Compared to Microcrystalline h-BN and c-BN. *Phys. Status Solidi C* **2005**, *2*, 318–321.
8. Tang, C.; Bando, Y.; Zhi, C. Y.; Golberg, D. Boron-Oxygen Luminescence Centres in Boron-Nitrogen Systems. *Chem. Commun.* **2007**, 4599–4601.
9. Museur, L.; Anglos, D.; Petitet, J.-P.; Michel, J.-P.; Kanaev, A. V. Photoluminescence of Hexagonal Boron Nitride: Effect of Surface Oxidation Under UV-Laser Irradiation. *J. Lumin.* **2007**, *127*, 595–600.
10. Pong, W. F.; Yueh, C. L.; Chang, Y. D.; Tsai, M. H.; Chang, Y. K.; Chen, Y. Y.; Lee, J. F.; Wei, S. L.; Wen, C. Y.; Chen, L. C.; et al. X-ray Absorption Studies of Carbon-Related Materials. *J. Synchrotron Radiat.* **2001**, *8*, 145–149.
11. Zhou, X.; Sham, T.-K.; Zhang, W.; Chan, C.-Y.; Bello, I.; Lee, S.-T.; Hofsaess, H. Cubic Phase Content and Structure of BN Films from an X-ray Absorption Study. *Anal. Chem.* **2006**, *78*, 6314–6319.

12. Zhou, X. T.; Sham, T. K.; Zhang, W. J.; Chan, C. Y.; Bello, I.; Lee, S. T.; Hofsass, H. X-ray Absorption Studies on Cubic Boron Nitride Thin Films. *J. Appl. Phys.* **2007**, *101*, 013710.
13. Hemraj-Benny, T.; Banerjee, S.; Sambasivan, S.; Fischer, D. A.; Han, W.; Misewich, J. A.; Wong, S. S. Investigating the Structure of Boron Nitride Nanotubes by Near-Edge X-ray Absorption Fine Structure (NEXAFS) Spectroscopy. *Phys. Chem. Chem. Phys.* **2005**, *7*, 1103–1106.
14. Sham, T. K.; Jiang, D. T.; Coulthard, I.; Lorimer, J. W.; Feng, X. H.; Tan, K. H.; Frigo, S. P.; Rosenberg, R. A.; Houghton, D. C.; Bryskiewicz, B. Origin of Luminescence from Porous Silicon Deduced by Synchrotron-Light-Induced Optical Luminescence. *Nature* **1993**, *363*, 331–334.
15. Sham, T. K.; Naftel, S. J.; Kim, P. S. G.; Sammynaiken, R.; Tang, Y. H.; Coulthard, I.; Moewes, A.; Freeland, J. W.; Hu, Y. F.; Lee, S. T. Electronic Structure and Optical Properties of Silicon Nanowires: A Study Using X-ray Excited Optical Luminescence and X-ray Emission Spectroscopy. *Phys. Rev. B* **2004**, *70*, 045313.
16. Han, W.-Q.; Yu, H.-G.; Zhi, C.; Wang, J.; Liu, Z.; Sekiguchi, T.; Bando, Y. Isotope Effect on Band Gap and Radiative Transitions Properties of Boron Nitride Nanotubes. *Nano Lett.* **2008**, *8*, 491–494.
17. Terauchi, M.; Tanaka, M.; Matsumoto, T.; Saito, Y. Electron Energy-Loss Spectroscopy Study of the Electronic Structure of Boron Nitride Nanotubes. *J. Electron Microsc.* **1998**, *47*, 319–324.
18. MacNaughton, J. B.; Moewes, A.; Wilks, R. G.; Zhou, X. T.; Sham, T. K.; Taniguchi, T.; Watanabe, K.; Chan, C. Y.; Zhang, W. J.; Bello, I.; et al. Electronic Structure of Boron Nitride Single Crystals and Films. *Phys. Rev. B* **2005**, *72*, 195113.
19. Troger, L.; Arvanitis, D.; Baberschke, K.; Michaelis, H.; Grimm, U.; Zschech, E. Full Correction of the Self-Absorption in Soft-Fluorescence Extended X-ray-Absorption Fine Structure. *Phys. Rev. B* **1992**, *46*, 3283–3289.
20. Choi, H. C.; Bae, S. Y.; Jang, W. S.; Park, J.; Song, H. J.; Shin, H.-J. X-ray Absorption Near Edge Structure Study of BN Nanotubes and Nanothorns. *J. Phys. Chem. B* **2005**, *109*, 7007–7011.
21. Tang, C.; Bando, Y.; Sato, T.; Kurashima, K. A Novel Precursor for Synthesis of Pure Boron Nitride Nanotubes. *Chem. Commun.* **2002**, 1290–1291.
22. Gou, G.; Pan, B.; Shi, L. The Nature of Radiative Transition in O-Doped Boron Nitride Nanotubes. *J. Am. Chem. Soc.* **2009**, *131*, 4839–4845.
23. Reshchikov, M. A.; Morkoc, H. Luminescence Properties of Defects in GaN. *J. Appl. Phys.* **2005**, *97*, 061301.
24. Wu, J.; Han, W.-Q.; Walukiewicz, W.; Ager, J. W., III; Shan, W.; Haller, E. E.; Zettl, A. Raman Spectroscopy and Time-Resolved Photoluminescence of BN and $B_xC_yN_z$ Nanotubes. *Nano Lett.* **2004**, *4*, 647–650.
25. Zhi, C.; Bando, Y.; Tang, C.; Golberg, D.; Xie, R.; Sekigushi, T. Phonon Characteristics and Cathodoluminescence of Boron Nitride Nanotubes. *Appl. Phys. Lett.* **2005**, *86*, 213110.
26. Dong, Z.; Song, Y. Transformation of Cold-Compressed Multiwalled Boron Nitride Nanotubes Probed by Infrared Spectroscopy. *J. Phys. Chem. C* **2010**, *114*, 1782–1788.
27. Gurr, G. E.; Montgomery, P. W.; Knutson, C. D.; Gorres, B. T. Crystal Structure of Trigonal Diboron Trioxide. *Acta Crystallogr., B* **1970**, *26*, 906–915.
28. Geick, R.; Perry, C. H.; Rupprecht, G. Normal Modes in Hexagonal Boron Nitride. *Phys. Rev.* **1966**, *146*, 543–547.
29. Zhi, C.; Bando, Y.; Tan, C.; Golberg, D. Effective Precursor for High Yield Synthesis of Pure BN Nanotubes. *Solid State Commun.* **2005**, *135*, 67–70.
30. Hu, Y. F.; Zuin, L.; Wright, G.; Igarashi, R.; McKibben, M.; Wilson, T.; Chen, S. Y.; Johson, T.; Maxwell, D.; Yates, B. W.; et al. Commissioning and Performance of the Variable Line Spacing Plane Grating Monochromator Beamline at the Canadian Light Source. *Rev. Sci. Instrum.* **2007**, *78*, 083109.
31. Regier, T.; Paulsen, J.; Wright, G.; Coulthard, I.; Tan, K.; Sham, T. K.; Blyth, R. I. R. Commissioning of the Spherical Grating Monochromator Soft X-ray Spectroscopy Beamline at the Canadian Light Source. *AIP Conf. Proc.* **2007**, *879*, 473–476.
32. Rosenberg, R. A.; Simons, J. K.; Frigo, S. P.; Tan, K.; Chen, J. M. X-ray Fluorescence Detection of Low-Z Elements Using a Microchannel Plate Detector. *Rev. Sci. Instrum.* **1992**, *63*, 2193–2194.